Anal. Chem. **2007,** *79,* 5574−5581

CdS Nanocrystal-Based Electrochemiluminescence Biosensor for the Detection of Low-Density Lipoprotein by Increasing Sensitivity with Gold Nanoparticle Amplification

Guifen Jie, Bo Liu, Hongcheng Pan, Jun-Jie Zhu,* and Hong-Yuan Chen

Key Laboratory of Analytical Chemistry for Life Science (Ministry of Education of China), School of Chemistry and Chemical Engineering, Nanjing University, Nanjing 210093, P. R. China

Mercaptoacetic acid (RSH)-capped CdS nanocrystals (NCs) was demonstrated to be electrochemically reduced during potential scan and react with the coreactant $S_2O_8^{2-}$ to generate strong electrochemiluminescence (ECL) in aqueous solution. Based on the ECL of CdS NCs, a novel label-free ECL biosensor for the detection of low-density lipoprotein (LDL) has been developed by using self-assembly and gold nanoparticle amplification techniques. The biosensor was prepared as follows: The gold nanoparticles were first assembled onto a cysteamine monolayer on the gold electrode surface. This gold nanoparticle-covered electrode was next treated with cysteine and then reacted with CdS NCs to afford a CdS NC-electrode. Finally, apoB-100 (ligand of LDL receptor) was covalently conjugated to the CdS NC-electrode. The modification procedure was characterized by cyclic voltammetry, electrochemical impedance spectroscopy, and atomic force microscopy, respectively. The resulting modified electrode was tested as ECL biosensor for LDL detection. The LDL concentration was measured through the decrease in ECL intensity resulting from the specific binding of LDL to apoB-100. The ECL peak intensity of the biosensor decreased linearly with LDL concentration in the range of 0.025−16 ng mL^{-1} with a detection limit of 0.006 ng mL^{-1}. The CdS NCs not only showed high ECL intensity and good biocompatibility but also could provide more binding sites for apoB-100 loading. In addition, the gold nanoparticle amplification for protein ECL analysis was applied to the improvement of the detection sensitivity. Thus, the biosensor exhibited high sensitivity, good reproducibility, rapid response, and long-term stability.

In recent years, semiconductor nanocrystals (NCs) with excellent luminescent properties have attracted increased attention because of its application in many areas of fundamental and technical importance.[1−3] Recent works have indicated the semiconductor NCs are electrically excitable in nonaqueous media[4−7] and aqueous systems[8] containing supporting electrolyte. Efficient and stable electrogenerated chemiluminescence (ECL) from CdSe NCs in aqueous solution can be obtained by applying a cathodic potential to the CdSe nanocrystal films.[8] The electrochemically reduced and oxidized Si NCs[4] or CdSe NCs[5] can react with the coreactants to generate ECL. Moreover, semiconductor quantum dots (QDs) have been widely used in bioconjugates[1,9−10] and optical biosensing.[11] Chan and Nie used water-soluble QDs as the biological labels.[2] Therefore, semiconductor NCs or QDs have great potential for development of novel ECL biosensors.

In addition, a rapid, highly specific method of detecting and quantifying biological substances is increasingly needed. These materials can be determined by a binding method with a high degree of specificity, such as antigen−antibody, nucleic acid hybridization, and protein−ligand. Electrochemical,[12,13] optical,[14] ECL,[15−22] and photoelectrochemical methods[23] have been used as special detection techniques. Among them, the ECL sensor

* Corresponding author. Tel: +86-25-83594976. Fax: +86-25-83317761. E-mail: jjzhu@netra.nju.edu.cn.

(1) Bruchez, M.; Moronne, M.; Gin, P.; Weiss, S.; Alivisatos, A. P. *Science* **1998**, *281*, 2013−2016.
(2) Chan, W. C. W.; Nie, S. M. *Science* **1998**, *281*, 2016−2018.
(3) Chen, S. W.; Truax, L. A.; Sommers, J. M. *Chem. Mater.* **2000**, *12*, 3864−3870.
(4) Ding, Z.; Quinn, B. M.; Haram, S. K.; Pell, L. E.; Korgel, B. A.; Bard, A. J. *Science* **2002**, *296*, 1293−1297.
(5) Myung, N.; Ding, Z.; Bard, A. J. *Nano Lett.* **2002**, *2*, 1315−1319.
(6) Myung, N.; Bae, Y.; Bard, A. J. *Nano Lett.* **2003**, *3*, 1053−1055.
(7) Bae, Y.; Myung, N.; Bard, A. J. *Nano Lett.* **2004**, *4*, 1153−1161.
(8) Poznyak, S. K.; Talapin, D. V.; Shevchenko, E. V.; Weller, H. *Nano Lett.* **2004**, *4*, 693−698.
(9) Wang, D.; Rogach, A. L.; Caruso, F. *Nano Lett.* **2002**, *2*, 857−861.
(10) Ding, S. Y.; Jones, M.; Tucker, M. P.; Nedeljkovic, J. M.; Wall, J.; Simon, M. N.; Rumbles, G.; Himmel, M. E. *Nano Lett.* **2003**, *3*, 1581−1585.
(11) Sapsford, K. E.; Medintz, I. L.; Golden, J. P.; Deschamps, J. R.; Uyeda, H. T.; Mattoussi, H. *Langmuir* **2004**, *20*, 7720−7728.
(12) Mikkelsen, S. R. *Electroanalysis* **1996**, *8*, 15−19.
(13) Wang, J. *Anal. Chim. Acta* **2002**, *469*, 63−71.
(14) Christodoulides, N.; Tran, M.; Floriano, P. N.; Rodriguez, M.; Goodey, A.; Ali, M.; Neikirk, D.; McDevitt, J. T. *Anal. Chem.* **2002**, *74*, 3030−3036.
(15) Lee, W. Y. *Mikrochim. Acta* **1997**, *127*, 19−39.
(16) Fähnrich, K. A.; Pravda, M.; Guilbault, G. G. *Talanta* **2001**, *54*, 531−559.
(17) Miao, W. J.; Bard, A. J. *Anal. Chem.* **2003**, *75*, 5877−5885.
(18) Namba, Y.; Usami, M.; Suzuki, O. *Anal. Sci.* **1999**, *15*, 1087−1093.
(19) Knight, A. W.; Greenway, G. M. *Analyst* **1995**, *120*, 2543−2747.
(20) Xu, X. H.; Jeffers, R. B.; Gao, J.; Logan, B. *Analyst* **2001**, *126*, 1285−1292.
(21) Zhou, M.; Roovers, J.; Robertson, G. P.; Grover, C. P. *Anal. Chem.* **2003**, *75*, 6708−6717.
(22) Richter, M. M. *Chem. Rev.* **2004**, *104*, 3003−3036.

10.1021/ac062357c CCC: $37.00
Published on Web 07/06/2007

has been paid much attention and proven to be a remarkable detector.[24,25] ECL sensors can not only retain the advantages of chemiluminescence (CL) sensors, such as the excellent sensitivity and a wide dynamic concentration response range, but also own some additional advantages over the CL sensors.[26−30] First, the application of potential can control the CL reaction and improve its selectivity; second, the generation of light in the vicinity of the electrode gives improved spatial control for sensitive detection; third, the target molecules can be electrochemically modified to form a CL-active species and extend its analytical application. Based on these advantages, both $Ru(bpy)_3^{2+}$ and luminol ECL have been widely applied to ECL sensors.[31,32] However, the bioanalysis based on [$Ru(bpy)_3^{2+}$] or luminol ECL possesses some limitations. Ruthenium labeling at multiple sites may result in the loss of biological activity of the molecules,[33,34] while luminol ECL is weak in neutral solution.[35] Therefore, the application of semiconductor nanocrystals to ECL biosensing is complementary and in some cases may be superior to existing ECL analysis. Moreover, the development of a NC-based ECL biosensor will open up a new perspective for the use of semiconductor NCs, which is of great significance for biological analysis.

The detection of low-density lipoprotein (LDL) is of particular importance, as LDL is most closely associated with heart disease.[36] LDL is the major cholesterol carrier in the blood stream and delivers exogenous cholesterol to cells by endocytosis.[37] The accumulation of LDL is regarded as the first stage of atherosclerotic lesions, so it is necessary to develop a biosensor for LDL detection. However, up to now, only Shannon and David introduced dextran sulfate (DS) to fabricate an acoustic wave biosensor for LDL detection,[38] but they were unable to achieve the same reproducibility for coating DS onto a similar surface, and the biosensor became a complicated case to treat theoretically.[38] ApoB-100, a ligand for the LDL receptor,[39] is a very large glycoprotein consisting of a single large polypeptide chain of 4536 amino acid residues with a molar mass of 514 kDa.[40,41] According to the report,[38] the critical step in LDL detection is the selective separation of LDL from the lipoprotein fractions. Here, the enhanced selectivity for the LDL detection was achieved by introducing the specific apoB-100−LDL interaction,[42] a model system for ligand−receptor binding, to the fabrication of a LDL biosensor.

In this paper, we explored ECL property of the water-soluble CdS NCs and developed a novel NCs ECL biosensor for LDL detection via self-assembly and nanoparticle amplification techniques. A gold nanoparticle layer was first conjugated to the electrode surface, and then CdS NCs and apoB-100 were directly immobilized onto the electrode. After the specific binding of apoB-100 with LDL, the biosensor underwent less ECL reaction due to the increased steric hindrance. As a result, ECL signals related to LDL concentration were measured. Because the gold nanoparticles and CdS NCs could provide more binding sites, the apoB-100 adsorption capacity could be much improved, and thus, the detection sensitivity was enhanced. To the best of our knowledge, no report on an ECL biosensor prepared by using ECL of semiconductor NCs coupled with a biospecific interaction has been found. This method is rapid, cost-effective, specific, and ultrasensitive for bioassays. The development of nanocrystals for an ECL biosensor may intrigue researchers into gaining a new interest in investigating the ECL property of semiconductor NCs with different shapes, sizes, and constitutions and promote the step of exploiting more applications of NCs ECL in bioassays.

EXPERIMENTAL SECTION

Reagents. Low-density lipoprotein (6.7 mg mL^{-1}) and apolipoprotein B-100 (4.8 mg mL^{-1}) were obtained from Nanjing Huibiao Biological Technology Co. Blood samples from fasting healthy donors were taken into polypropylene tubes containing ethylenediaminetetraacetate (EDTA; final concentration 1 mg of EDTA/mL of blood) and processed within 2 h. During this period, they were kept in semidarkness. Plasma was obtained by centrifugation at 2500*g* for 6 min. The LDL was isolated from fresh human plasma by differential ultracentrifugation and dialyzed against 50 mM phosphate buffer, pH 7.4, with 0.15 M NaCl and 0.1 mM EDTA at 4 °C for 24 h. After sterilization, the standard LDL stock solutions were prepared with PBS (pH 7.4) and stored at 4 °C. ApoB-100 fragments were generated by digestion of LDL (1 mg) with thrombin (enzyme/substrate 1:100 w/w) for 36 h at room temperature. *N*-Hydroxysuccinimide (NHS) and bovine serum albumin (BSA, 96−99%) were obtained from Sigma (St. Louis, MO). 1-Ethyl-3-(3-dimethylaminopropyl) carbodiimide hydrochloride (EDC) was purchased from Pierce (Rockford, IL). $HAuCl_4 \cdot 4H_2O$ (48% w/w) and $K_2S_2O_8$ were purchased from Shanghai Chemical Reagent Co. (Shanghai, China). The 0.1 M PBS (pH 7.4) containing 0.1 M $K_2S_2O_8$ and 0.1 M KCl was used as the electrolyte in the measuring system. Doubly distilled water was used throughout.

Apparatus. The electrochemical measurement for ECL was carried out on a CHI 812 electrochemical working station (Shanghai CH Instruments Co.) using a three-electrode system.

(23) Dong, D.; Zheng, D.; Wang, F. Q.; Yang, X. Q.; Wang, N.; Li, Y. G.; Guo, L. H.; Cheng, J. *Anal. Chem.* **2004**, *76*, 499−501.
(24) Chi, Y.; Duan, J.; Lin, S.; Chen, G. *Anal. Chem.* **2006**, *78*, 1568−1573.
(25) Du, Y.; Wei, H.; Kang, J.; Yan, J.; Yin, X.; Yang, X. R.; Wang, E. K. *Anal. Chem.* **2005**, *77*, 7993−7997.
(26) Knight, A. W. *Trends Anal. Chem.* **1999**, *18*, 47−62.
(27) Knight, A. W.; Greenway, G. M. *Analyst* **1994**, *119*, 879−890.
(28) Richter, M. M. *Chem. Rev.* **2004**, *104*, 3003−3036.
(29) Zu, Y. B.; Ding, Z. F.; Zhou, J. F.; Lee, Y. M.; Bard, A. J. *Anal. Chem.* **2001**, *73*, 2153−2156.
(30) Buck, S. M.; Xu, H.; Brasuel, M.; Philbert, M. A.; Kopelman, R. *Talanta* **2004**, *63*, 41−59.
(31) Zhan, W.; Alvarez, J.; Crooks, R. M. *Anal. Chem.* **2003**, *75*, 313−318.
(32) Qi, H. L.; Zhang, C. X. *Anal. Chim. Acta* **2004**, *50*, 31−35.
(33) Zhou, M.; Roovers, J.; Robertson, G. P.; Grover, C. P. *Anal. Chem.* **2003**, *75*, 6708−6717.
(34) Zhou, M.; Roovers, J. *Macromolecules* **2001**, *34*, 244−252.
(35) Fähnrich, K. A.; Pravda, M.; Guibault, G. G. *Talanta* **2001**, *54*, 531−559.
(36) Havel, R. J.; Kane, J. P. In *The Metabolic Basis of Inherited Disease,* 6th ed.; Scriver, C. R., Beaudet, A. L., Sly, W. S., Valle, D., Eds.; McGraw-Hill: New York, 1989; Chapter 44A.
(37) Goldstein, J. L.; Brown, M. S. *Annu. Rev. Biochem.* **1977**, *46*, 897−930.
(38) Snellings, S.;Fuller, J.; Pitner, M; David, P. W. *Biosens. Bioelectron.* **2003**, *19*, 353−363.
(39) Schumaker, V. N.; Phillips, M. L.; Chatterton, J. E. *Adv. Protein Chem.* **1994**, *45*, 205−248.
(40) Knott, T. J.; Pease, R. J.; Powell, L. M.; Wallis, S. C.; Rall, S. C., Jr.; Innerarity, T. L.; Blackhart, B.; Taylor, W. H.; Marcel, Y.; Milne, R.; Johnson, D.; Fuller, M.; Lusis, A. J.; McCarthy, B. J.; Mahley, R. W.; Levy-Wilson, B.; Scott, J. *Nature* **1986**, *323*, 734−738.
(41) Yang, C. Y.; Chen, S. H.; Gianturco, S. H.; Bradley, W. A.; Sparrow, J. T.; Tanimura, M.; Li, W. H.; Sparrow, D. A.; DeLoof, H.; Rosseneu, M.; Lee, F. S.; Gu, Z. W.; Gotto, A. M., Jr; Chan, L. *Nature* **1986**, *323*, 738−742.
(42) Sommer, A.; Prenner, E.; Gorges, R.; Stütz, H.; Grillhofer, H.; Kostner, G. M.; Paltauf, F.; Hermetter, A. *J. Biol. Chem.* **1992**, *267*, 24217−24222.

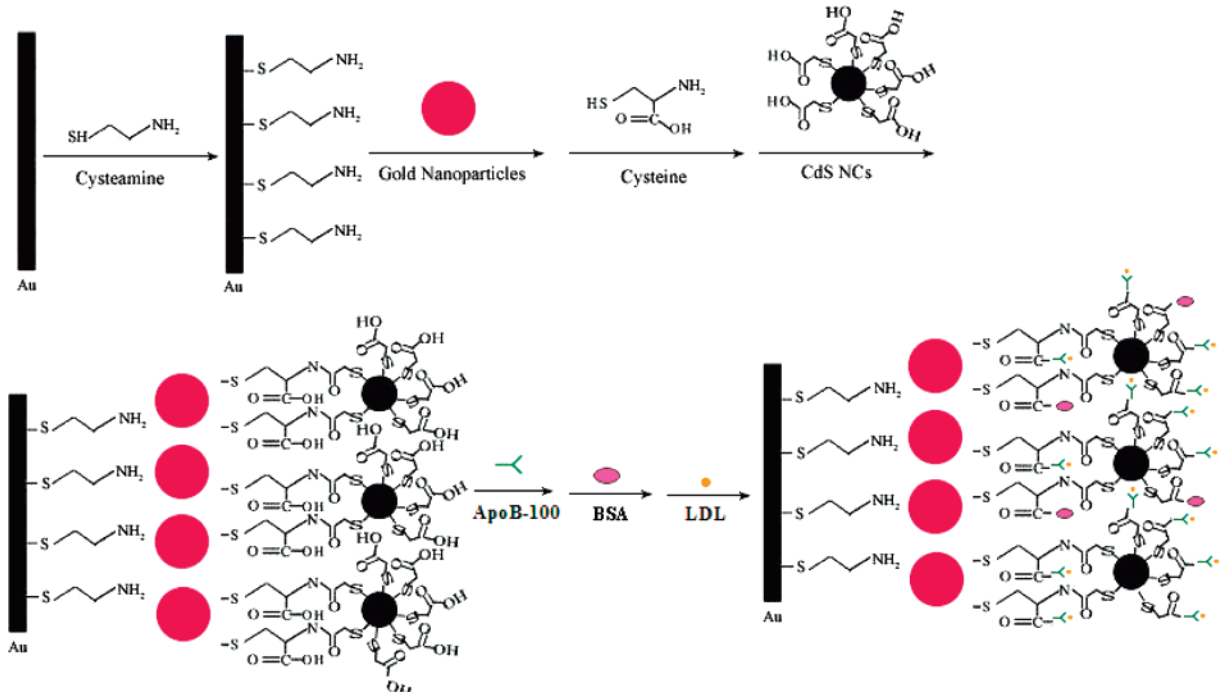

Figure 1. Schematic diagram for the biosensor fabrication and LDL binding.

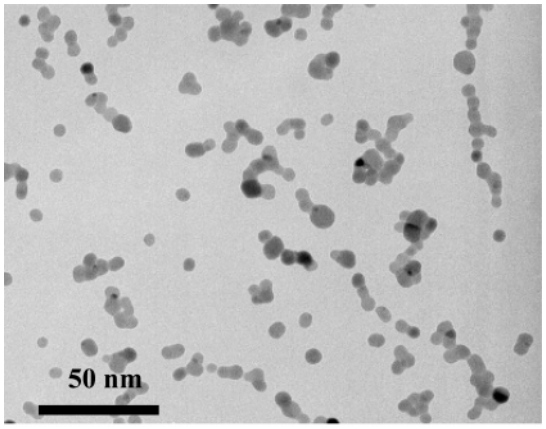

Figure 2. TEM image of the CdS NCs.

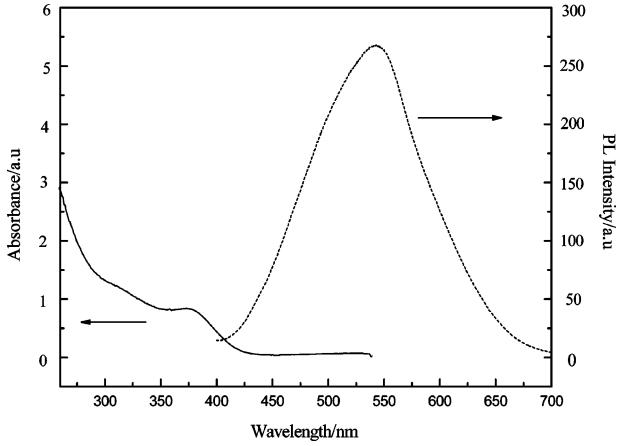

Figure 3. PL and UV spectra of the CdS NCs in 0.1 M PBS (pH 7.4). Excitation wavelength, 380 nm.

The electrodes were a 4-mm-diameter Au disk working electrode, a saturated calomel reference electrode (SCE), and a Pt counter electrode. The ECL emission was detected with a model MPI-A electrochemiluminescence analyzer (Xi'An Remax Electronic Science & Technology Co. Ltd., Xi'An, China) at room temperature. The spectral width of the photomultiplier tube (PMT) was 200−800 nm, and the voltage of the PMT was set at 800 V in the process of detection. Cyclic voltammetry and electrochemical impedance spectroscopy (EIS) were carried out with a CHI 660A electrochemical working station (Shanghai CH Instruments Co.), using the same three-electrode system as that in the ECL detection. UV absorption spectra were acquired with a Ruili 1200 photospectrometer (Peking Analytical Instrument Co., Peking, China). Photoluminescence (PL) spectra were obtained on an RF-540 spectrophotometer (Shimadzu). Atomic force micrograph (AFM) was operated in tapping mode in air and at room temperature. Images were acquired at a scan rate of 1.5 Hz with a Seiko Spi3800N atomic force microscope (Seiko). The AFM tip force constant was 40 N/m, and the AFM was calibrated.

The transmission electron microscope (TEM) image of the CdS NCs was carried out on a TEM (Jeol JEM-200CX) operating at an acceleration voltage of 100 kV. The colloidal particle solution was dropped on a carbon-coated copper grid, after which the grid was allowed to dry at room temperature before TEM imaging. Each spot corresponds to an individual particle (only the inorganic cores have enough contrast to be visualized by TEM).

Preparation of Gold Nanoparticles. Gold nanoparticles were prepared according to the ref 43. A 100-mL solution containing 0.01 g of $HAuCl_4 \cdot 4H_2O$ was brought to reflux and then 3 mL of 1% sodium citrate solution was introduced while stirring. The solution was then kept boiling for another 40 min and left to cool to room temperature. The resulting gold particle has a diameter of 24 nm.

Preparation of Water-Soluble CdS NCs. Mercaptoacetic acid-capped CdS NCs were prepared according to the literature.[44]

(43) Frens, G. *Nat. Phys. Sci.* **1973**, *241*, 20−22.

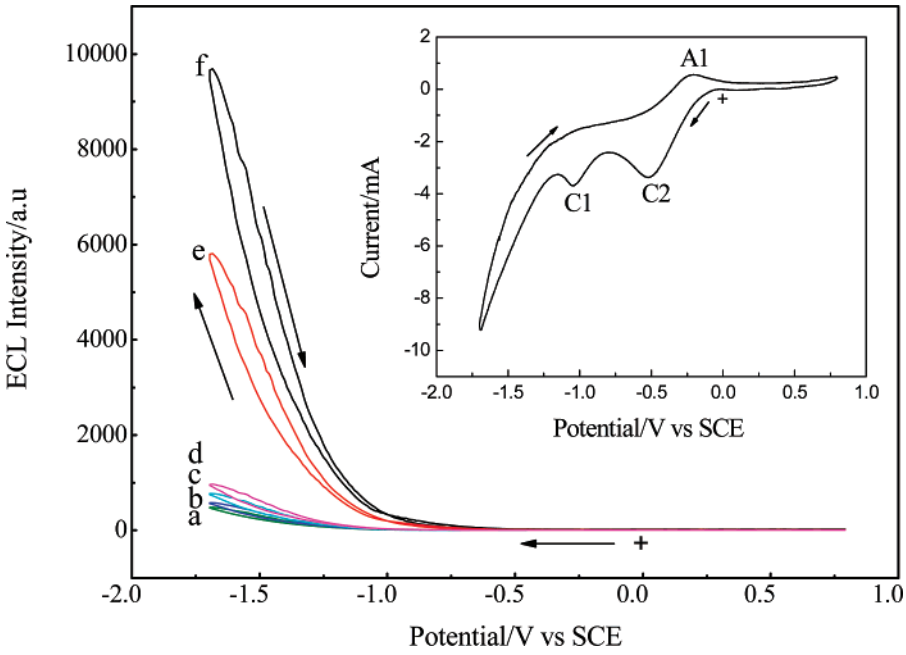

Figure 4. Electrochemiluminescence intensity versus potential. (a) On the bare Au electrode; (b) on the cysteamine/Au electrode; (c) on the gold nanoparticles/cysteamine/Au electrode; (d) on the cysteine/gold nanoparticles/cysteamine/Au electrode; (e) on the CdS NCs/cysteine/Au electrode; (f) on the CdS NCs/cysteine/gold nanoparticles/cysteamine/Au electrode. Inset: cyclic voltammogram on the CdS NCs/cysteine/gold nanoparticles/cysteamine/Au electrode. 0.1 M PBS (pH 7.4) containing 0.1 M $K_2S_2O_8$ and 0.1 M KCl. Scan rate, 100 mV s^{-1}.

A 2-μL sample of mercaptoacetic acid was added to 100 mL of 1 mmol L^{-1} cadmium chloride solution under vigorous stirring, and the pH was adjusted to ~11 with 0.5 mol L^{-1} NaOH. The solution was bubbled with nitrogen for 30 min, and 50 mL of 1.34 mmol L^{-1} Na_2S was added dropwise to the solution. The reaction was kept under bubbling nitrogen for 24 h. The resulting nanoparticle has an average diameter of 10 nm.

Fabrication of the ECL Biosensor. A gold disk electrode with a diameter of 4 mm was polished carefully with 1.0-, 0.3-, and 0.05-μm α-Al_2O_3 powder on fine abrasive paper and washed ultrasonically with water and absolute ethanol. Before modification, the bare electrode was scanned in 0.5 M H_2SO_4 between 0.3 and 1.5 V until a reproducible cyclic voltammogram (CV) was obtained. After cleaning, the electrode was first immersed into 0.02 mol L^{-1} deoxygenated cysteamine aqueous solution for 20 h in darkness at room temperature. Then, the electrode was rinsed thoroughly with redistilled water and dipped into the colloidal gold at 4 °C for 10 h. To assemble the CdS NCs onto the electrode, the gold nanoparticle-modified electrode was immersed in 0.02 mol L^{-1} cysteine solution at 4 °C for 20 h, followed by soaking in 40 μL of 0.05 mM CdS NCs containing 20 mg mL^{-1} EDC at 4 °C for 10 h. And then, for the immobilization of apoB-100, the resulting electrode was incubated in 40 μL of 500 μg mL^{-1} apoB-100 containing 20 mg mL^{-1} EDC and 10 mg mL^{-1} NHS at 4 °C for 12 h. Finally, 20 μL of 0.2 wt % BSA was dropped on the electrode at 37 °C for 1 h to block nonspecific binding sites of the CdS NCs. For the binding of LDL, the biosensor was incubated in different concentrations of LDL at 37 °C for 45 min.

Figure 1 outlines the steps of fabricating the ECL biosensor and binding of LDL, including cysteamine self-assembled on Au electrode, a gold nanoparticle layer conjugated to cysteamine, the carboxyl group functionalized CdS NCs covalently attached on the cysteine, apoB-100 cross-linked on CdS NCs, BSA used to block nonspecific binding sites of the CdS NCs, and, finally, LDL specifically bound with apoB-100.

ECL Detection of LDL. The corresponding electrode above was in contact with 0.1 M PBS (pH 7.4) containing 0.1 M $K_2S_2O_8$ and 0.1 M KCl and scanned from 0.8 to −1.7 V. ECL signals related to the LDL concentrations were measured.

RESULTS AND DISCUSSION

Nanoparticle Characterization. Figure 2 showed the TEM image of the CdS NCs. Both the gray and black dots correspond to the CdS nanoparticles. The formation of the black dots is due to the overlap of the gray dots. According to the TEM observation, the average size of the CdS nanoparticles is ~10 nm and their size distribution is relatively uniform.

PL and Absorption Spectra of CdS Nanocrystals. Photoluminescence and absorption spectra are used to characterize the CdS NCs. Figure 3 showed the PL and absorption spectra of the mercaptoacetic acid-capped CdS NCs in 0.1 M PBS (pH 7.4). The PL emission peak at 541 nm (λ_{ex} = 380 nm) and absorption maximum at 374 nm indicated the consequence of quantum confinement.[44] According to the literature,[45] the particle size could also be calculated in virtue of the following expression:

$$D = (-6.6521 \times 10^{-8})\lambda^3 + (1.9557 \times 10^{-4})\lambda^2 - (9.2352 \times 10^{-2})\lambda + 13.29$$

λ is the UV peak (374 nm); the result shows that the particle diameter of the as-prepared CdS NCs is ~10 nm, which is consistent with the result of the TEM.

(44) Jiang, L.; Chen, X.; Yang, W. S.; Jin, J.; Yang, B. Q.; Xu, L; Li, T. J. *Chem. J. Chin. Univ.* **2001**, *22*, 1397−1399.

(45) Yu, W. W.; Qu, L.; Guo, W.; Peng, X. *Chem. Mater.* **2003**, *15*, 2854−2860.

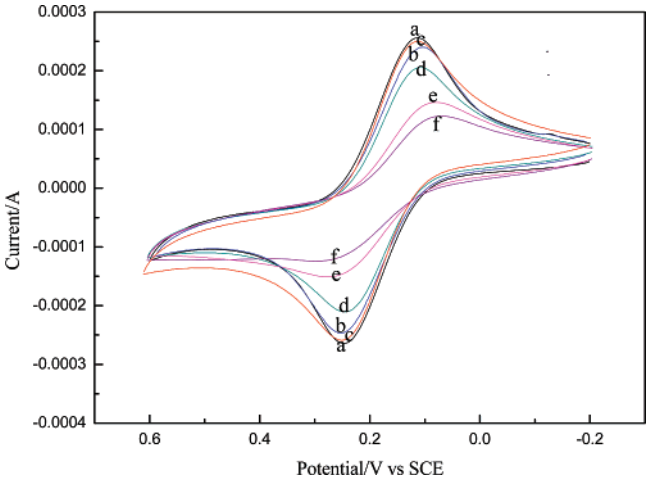

Figure 5. Cyclic voltammograms of the electrode at different stages. (a) on the bare Au electrode surface, (b) on the cysteamine-modified Au electrode surface, (c) on the gold nanoparticles surface, (d) on the CdS NCs surface, (e) on the apoB-100 surface, and (f) on the apoB-100 +BSA surface. Supporting electrolyte: 10 mM PBS (2.5 mM $Fe(CN)_6^{4-/3}$ + 0.1 M KCl, pH 7.4), scan rate: 100 mV s^{-1}.

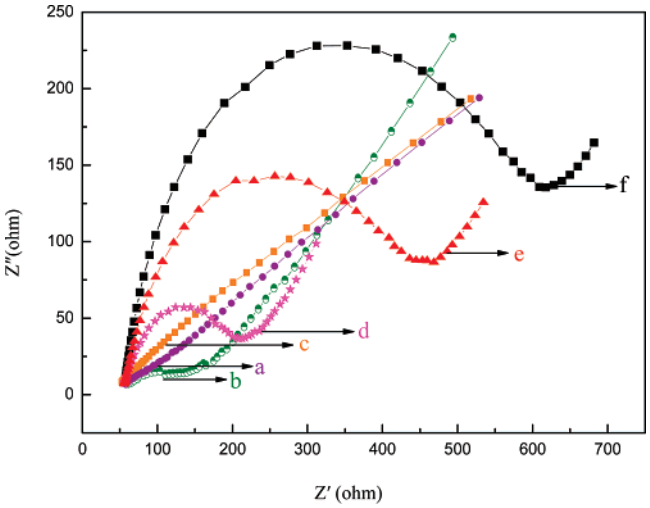

Figure 6. EIS of the electrode at different stages in 10 mM PBS (2.5 mM $Fe(CN)_6^{4-/3-}$ + 0.1 M KCl, pH 7.4) (a) on the bare Au electrode surface, (b) on the cysteamine-modified Au electrode surface, (c) on the gold nanoparticles surface, (d) on the CdS NCs surface, (e) on the apoB-100 surface, and (f) on the apoB-100 +BSA surface. The frequency range is between 1 and 10 000 Hz with signal amplitude of 5 mV.

Electrochemical and ECL Behaviors of the CdS Nanocrystals. Figure 4 (inset) showed the CVs of CdS NCs on the gold nanoparticle-modified Au electrode in 0.1 M PBS (pH 7.4) containing 0.1 M $K_2S_2O_8$ and 0.1 M KCl. Two cathodic peaks (C1, C2) and one anodic (A1) peak were observed at −1.05, −0.52, and −0.22 V, respectively. Among them, C1, corresponding to the reduction of CdS NCs, did not appear on the gold nanoparticle-modified electrode without CdS NCs. C2 was attributed to the reduction of $S_2O_8^{2-}$. A1 was probably involved in the oxidation of OOH^- produced by dissolved oxygen.[46]

Figure 4 showed the ECL curves of CdS NCs on the bare Au electrode (e) and on the gold nanoparticle-modified Au electrode (f) in 0.1 M PBS (pH 7.4) containing 0.1 M $K_2S_2O_8$ and 0.1 M KCl. In both curves, one ECL peak was observed at −1.68 V (ECL-1), resulting from the reaction between CdS NCs and $S_2O_8^{2-}$. It is highlighted that the ECL intensity of CdS NCs on the bare Au electrode was enhanced by ~1.6 orders of magnitude on the gold nanoparticle-modified electrode, which demonstrated that the gold nanoparticles could amplify ECL signal of CdS NCs.

To gain a better understanding of the ECL generation, we also performed the experiments in the absence of CdS NCs. As shown in Figure 4a−d, they were the ECL profiles of the bare Au electrode, the cysteamine/Au electrode, the gold nanoparticles/cysteamine/Au electrode, and the cysteine/gold nanoparticles/cysteamine/Au electrode, respectively. It could be found that all the background ECL signals from the Au electrode without CdS NCs were very low, indicating that the cysteamine, cysteine, and gold nanoparticles could not generate ECL. Thus, ECL was from the CdS NCs.

According to the report, the electrochemically reduced and oxidized Si NCs[4] or CdSe NCs[5] can react with the coreactants to produce ECL. In this case, upon the potential scan with an initial negative direction, the CdS NCs immobilized on the electrode were reduced to nanocrystal species ($CdS^{-\bullet}$) by charge injection,[5] while the coreactant $S_2O_8^{2-}$ was reduced to the strong oxidant $SO_4^{-\bullet}$, and then $CdS^{-\bullet}$ could react with $SO_4^{-\bullet}$ to emit light in the aqueous solution. According to the literature,[5,47] the coreactant can also be dissolved oxygen or H_2O_2. The corresponding ECL processes are as follows:[5]

$$CdS\ NCs + ne \rightarrow nCdS^{-\bullet} \quad (1)$$

$$S_2O_8^{2-} + e^- \rightarrow SO_4^{2-} + SO_4^{-\bullet} \quad (2)$$

$$CdS^{-\bullet} + SO_4^{-\bullet} \rightarrow CdS^* + SO_4^{2-} \quad (3)$$

$$CdS^* \rightarrow CdS + h\nu \quad (4)$$

$$O_2 + H_2O + 2e \rightarrow OOH^- + OH^- \quad (5)$$

$$2CdS^{-\bullet} + OOH^- + H_2O \rightarrow 3OH^- + 2CdS^* \quad (6)$$

$$2CdS^{-\bullet} + H_2O_2 \rightarrow 2OH^- + 2CdS^* \quad (7)$$

$$CdS^* \rightarrow CdS + h\nu \quad (8)$$

Characterization of the Biosensor Fabrication. The cyclic voltammogram of ferricyanide is a valuable tool to monitor the barrier of the modified electrode, as electron transfer between the solution species and the electrode must occur by tunneling through the barrier. Therefore, it was chosen as a marker to investigate the changes of the electrode behavior after each assembly step. Figure 5 showed the cyclic voltammograms of $Fe(CN)_6^{4-/3-}$ at the Au electrode of different stages. As could be seen, when the electrode was first treated with cysteamine, the monolayer of cysteamine on the electrode led to a small decrease of peak current (curve b). However, when gold nanoparticles were deposited on the cysteamine-modified electrode, a slight increase in the amperometric response was observed (curve c). It is

(46) Cui, H.; Xu, Y.; Zhang, Z. F. *Anal. Chem.* **2004**, *76*, 4002−4010.

(47) Cui, H.; Zou, G. Z.; Lin, X. Q. *Anal. Chem.* **2003**, *75*, 324−331.

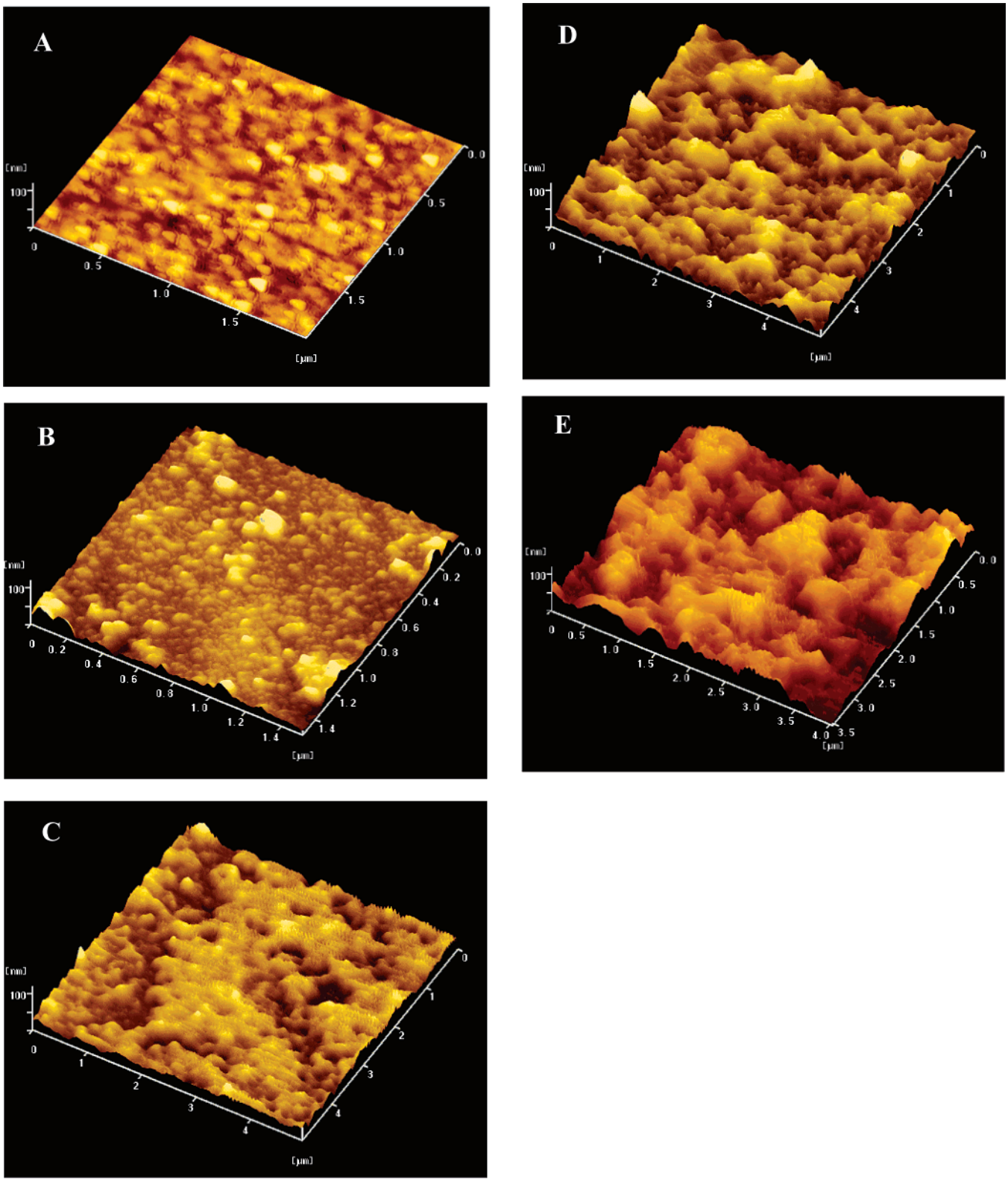

Figure 7. AFM images of Au electrode at different stages: (a) the bare Au electrode surface, (b) the gold nanoparticles surface, (c) the CdS NCs surface, (d) the apoB-100 surface, and (e) the apoB-100 +BSA surface.

reasonable that the gold nanoparticles can increase the effective surface area of the electrode and enhance the rate of electron transfer. And then CdS NCs were assembled on the gold nanoparticle-modified electrode, which partially blocked the electron transfer of the redox probe and resulted in a further decrease of CV. In particular, after apoB-100 was immobilized on the electrode, an obvious decrease in the peak current was obtained (curve d). The reason is that the apoB-100 molecules act as the inert electron and mass-transfer blocking layer and hinder the diffusion of ferricyanide toward the electrode surface. Finally, BSA was dropped on the electrode to block nonspecific binding sites of the CdS NCs surface, which remarkably increased

the insulating property of the resulting electrode and decreased the peak current (Figure 6, curve f).

EIS can also give further information on the impedance changes of the electrode surface in the modification process. In EIS, the semicircle diameter equals the electron-transfer resistance, R_{et}. This resistance controls the electron-transfer kinetics of the redox probe at the electrode interface. Curve a in Figure 6 showed the EIS of the bare Au electrode. An almost straight line was exhibited, which was characteristic of a mass diffusional limiting electron-transfer process. After the electrode was treated with cysteamine, the EIS of the assembled cysteamine monolayer showed a small interfacial *eT* resistance (Figure 6, curve b). And then, the gold nanoparticles were conjugated to the amine-modified surface. We were surprised to find that the EIS of the gold nanoparticle-modified electrode was similar to that of the bare Au electrode (Figure 6, curve c). The reason may be that the gold nanoparticles immobilized on the cysteamine monolayer play an important role similar to a conducting wire, which makes it easier for the electron transfer to take place. As for the assembly mechanism by Au−amine interaction, one opinion is that it is mainly by electrostatic adsorption between the negatively charged nano-Au particles and the protonated amines;[48] another opinion, however, postulates that there are strong covalent bonds between Au and amine.[49,50] Subsequently, CdS NCs were assembled on the gold nanoparticle-modified electrode and R_{et} increased a little (Figure 6, curve d). However, after apoB-100 was immobilized on the electrode, the interfacial resistance (Figure 6, curve e) remarkably increased. And R_{et} increased in the same way after BSA was dropped on the electrode surface (Figure 6, curve f). These results are consistent with the fact that the protein layer insulates the conductive support and perturbs the interfacial electron-transfer.

In addition, AFM technique was also employed to confirm the fabrication process of the biosensor. Figure 7A showed an image of the bare gold substrate, which possessed a homogeneous surface structure. The thickness of the pure gold film was ~6 nm. After gold nanoparticles were assembled onto the gold surface through cysteamine, the thickness of the layers increased to 40 nm (Figure 7B). From the topographic feature on the gold surface, the gold nanoparticles could also be observed. Figure 7C showed the AFM image of the CdS NCs layer immobilized onto the gold nanoparticles, and the thickness of all the layers increased to 50 nm. The surface morphology could be clearly distinguished from that in Figure 7B. When apoB-100 was immobilized onto the electrode, the thickness of all the layers increased to 70 nm (Figure 7D). The apoB-100 as an aggregated pattern was also observed. Figure 7E demonstrated the surface topographic image after BSA blocked nonspecific binding sites of the CdS NCs surface. The aggregates of BSA could be seen, and the thickness of all the layers became 90 nm.

On the basis of the CVs, EIS, and AFM results, we conclude that CdS NCs and apoB-100 have been successfully immobilized on the electrode surface, and thus, the biosensor has been fabricated.

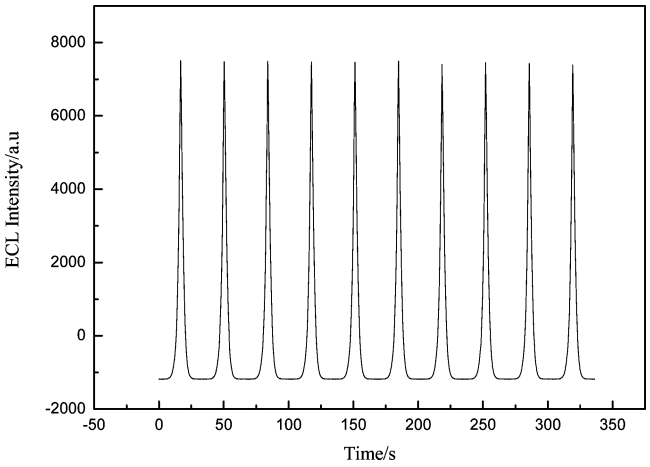

Figure 8. ECL emission from the biosensor in pH 7.4 PBS containing 0.1 M KCl and 0.1 M $K_2S_2O_8$ under continuous cyclic voltammetry for 10 cycles. Scan rate, 100 mV s^{-1}.

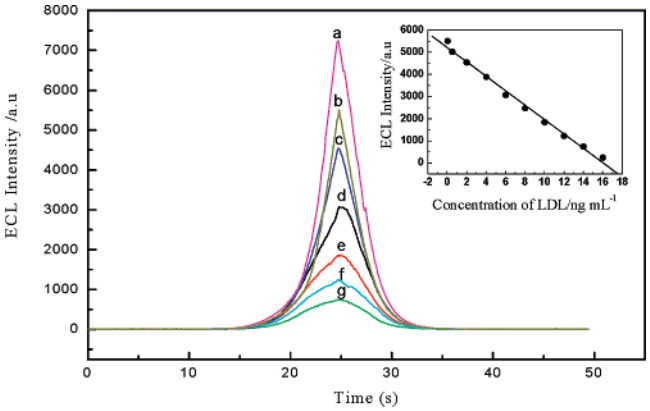

Figure 9. ECL profiles of the biosensor in the absence (a) and presence (b−g) of different concentrations of LDL in pH 7.4 PBS containing 0.1 M KCl and 0.1 M $K_2S_2O_8$. Inset: calibration curve for LDL determination. LDL concentration (ng mL^{-1}): (a) 0, (b) 0.025, (c) 2, (d) 6, (e) 10, (f) 12, and (g) 14. Scan rate, 100 mV s^{-1}.

ECL Characteristic of the Biosensor. Figure 8 showed the ECL emission from the biosensor under continuous potential scanning for 10 cycles. Stable and high ECL signals (7473) were observed, which suggested that the biosensor was suitable for ECL detection. Compared with Figure 4, the ECL intensity (7473) from the biosensor was found to be lower than that (9687) from the CdS NC-modified electrode. This could be explained by the additional immobilization of the apoB-100 and BSA on the electrode surface, which hindered the ECL reaction and resulted in the decrease in ECL intensity of the biosensor.

ECL Detection of LDL. Figure 9 showed the ECL intensity of the biosensor in the absence (a) and presence (b−g) of different concentrations of LDL. It could be seen that the ECL intensity in the presence of LDL (b) was lower than that in the absence of LDL (a), and the ECL intensity decreased gradually with increasing concentrations of LDL (b−g). The reason was that the specific binding of apoB-100 with LDL greatly inhibited the ECL reaction of CdS NCs on the electrode, and thus decreased the ECL intensity, which suggested that the LDL concentration could be

(48) Bar, G.; Rubin, S.; Cutts, R. W.; Taylor, T. N.; Zawodzinski, T. A. *Langmuir* **1996**, *12*, 1172−1179.
(49) Oison, L G.; Lo, Y .; Beebe, T. P.; Harris, J. M. *Anal. Chem.* **2001**, *73*, 4268−4276.
(50) Brown, K. R.; Fox, A. P.; Natan, M. J. *J. Am. Chem. Soc.* **1996**, *118*, 1154−1157.

determined by the ECL measurement of the biosensor.

The standard calibration curve for the LDL detection was shown in the inset of Figure 9. The ECL intensity decreased linearly with the LDL concentration from 0.025 to 16 ng mL^{-1} with a detection limit of 0.006 ng mL^{-1}. The linear equation was $I = 5210-324C$ (unit of C is ng mL^{-1}), and the correlation coefficient was 0.9962. According to the linear equation, we could detect LDL concentration quantitatively. Higher plasma LDL levels could be detected by an appropriate dilution with pH 7.4 PBS.

Precision, Reproducibility, and Stability of the Biosensor. The reproducibility of the biosensor for LDL was investigated with intra- and interassay precision. The intraassay precision of the biosensor was evaluated by assaying one LDL level for three replicate measurements. The interassay precision was estimated by determining one LDL level with three biosensors made at the same electrode. The intra- and interassay variation coefficients (CVs) obtained from 6 ng mL^{-1} LDL were 4.5 and 8.6%, respectively. Obviously, the interassay CV showed an acceptable reproducibility; while the low value of intra-assay CV indicated that the biosensor could be regenerated and used repeatedly.

After the biosensor was used for 20 times, the analytical performances did not show an obvious decline, demonstrating that the sensing layers of the biosensor possessed good stability.

Application of the Biosensor in Human LDL Levels. The plasma LDL levels in two samples were analyzed by using the biosensor. These two samples were first diluted to 6.0 and 8.0 ng mL^{-1}, respectively. According to the standard curve, the mean plasma LDL concentrations were determined to be 6.1 and 7.8 ng mL^{-1}, which were in acceptable agreement with the above results. The relative errors were 1.6 and 2.5%, respectively. Thus, the proposed biosensor could be satisfactorily applied to the clinical determination of LDL levels in human plasma.

CONCLUSIONS

This work demonstrated that the CdS NCs could be electrochemically reduced during potential scan and react with the coreactant $S_2O_8^{2-}$ to generate strong ECL in aqueous solution. Based on the ECL, a novel non-labeled ECL biosensor has been successfully fabricated by a self-assembly technique for LDL determination. The CV, EIS, and AFM have been used as powerful tools to characterize the fabrication process. The resulting ECL biosensor exhibits high sensitivity, good reproducibility, and long-term stability.

Several advantages of the proposed method should be highlighted. First, CdS NCs, one of the novel classes of semiconductor nanocrystals, were used to fabricate a novel ECL biosensor. The NCs not only showed high ECL intensity, good biocompatibility, and conductivity, but also functioned as an effective conjugate to provide a sufficient amount of sites for binding apoB-100 molecules. Second, the gold nanoparticle amplification for protein ECL analysis was used to improve the detection sensitivity. Third, CdS NCs and apoB-100 were firmly immobilized on the electrode surface for the strong interactions between carboxyl and amino groups. Fourth, combining high sensitivity of NCs ECL detection with specificity of ligand−receptor binding, the biosensor can become an alternative method to other bioassays.

ACKNOWLEDGMENT

We greatly appreciate the support of the National Natural Science Foundation of China for Distinguished Young Scholars (20325516), the Key Program (20635020, 90206037), Creative Research Group (20521503), and General Program (20575026, 90606016). This work is also supported by Jiangsu Scientific Foundation of China (BK2006114).

Received for review December 13, 2006. Accepted May 15, 2007.

AC062357C